Initiation and maturation of the early axonal βII-spectrin membrane-associated periodic skeleton requires active cytoskeletal remodelling

Shivani Bodas[1], Ashish Mishra[2], Pramod Pullarkat[2] and Aurnab Ghose[1,*]

[1] Indian Institute of Science Education and Research (IISER) Pune, Dr. Homi Bhabha Road, Pune 411008, India.

[2] Raman Research Institute, C. V. Raman Avenue, Bengaluru 560 080, India

[*] Correspondence: aurnab@iiserpune.ac.in

Running head: Development of the βII-spectrin membrane-associated periodic skeleton

Keywords: βII-spectrin; membrane-associated periodic skeleton (MPS); F-actin; microtubule; STED

ABSTRACT

The axonal membrane-associated periodic skeletal (MPS) consisting of evenly spaced F-actin rings crosslinked by spectrin heterotetramers has been observed in many neuronal subtypes across multiple species. The MPS has been implicated in a diversity of functions ranging from a load-bearing tension buffer to a periodic ruler positioning channels and signalling complexes. However, the initiation and early development of the axonal MPS are poorly understood.

Using superresolution imaging of embryonic dorsal root ganglion axons, we show that the early development of the βII-spectrin MPS involves recruitment and stabilisation of the βII-spectrin to the axonal cortex followed by progressive establishment of long-range periodic order. Microtubule dynamics are essential for MPS formation in the early stages, while microtubules have a passive stabilizing function in the mature MPS. We show that the early subplasmalemmal recruitment and confinement of βII-spectrin is dependent on cortical actin. Further, active nucleation of F-actin is required in early development but dispensable for the maintenance of the mature MPS. Finally, using a βII-spectrin knockout model, we demonstrate that the actin-binding and lipid interacting domains of βII-spectrin are critical for its subplasmalemmal confinement and, subsequently, MPS maturation.

Our study provides insights into the mechanisms governing the development and maturation of the axonal MPS, highlighting the critical role of cytoskeletal dynamics.

INTRODUCTION

The axonal subplasmalemmal membrane periodic skeleton (MPS) is ubiquitous across phyla and forms a quasi-1D lattice along the entire neuronal axon (D'Este *et al.*, 2016; He *et al.*, 2016). A similar scaffold is found in dendrites and dendritic spine necks (Han *et al.*, 2017). The MPS comprises of axially aligned tetramers of α and β spectrins that are attached to evenly distributed radial F-actin rings, which maintain a typical spacing of 180 – 190 nm (Xu *et al.*, 2013). The lattice acts as a load-bearing scaffold, providing mechanical support to the plasma membrane (Hammarlund *et al.*, 2007; Dubey *et al.*, 2020). The MPS plays an essential role in the maintenance of axonal homoeostasis, regulating the ion channel distribution, maintaining the axonal diameter and facilitating axonal transport (Costa *et al.*, 2020; Wang *et al.*, 2020). Furthermore, the MPS acts as a signalling scaffold (Zhou *et al.*, 2019) , limits diffusion at the AIS (Albrecht *et al.*, 2016), modulates endocytosis (Wernert *et al.*, 2024) and is linked to axon degeneration (Unsain *et al.*, 2018; Wang *et al.*, 2019). Studies in *C. elegans*, mice and humans have revealed that impairment of the MPS leads to a variety of defects and lethality(Hammarlund *et al.*, 2007; Huang *et al.*, 2017a, 2017b; Lorenzo *et al.*, 2019; Cousin *et al.*, 2021).

Despite the explosion of interest in the axonal MPS, its early development and maintenance is not well understood. Cytoskeleton dependence on MPS stability has been typically studied in late-stage neurons and does not address early functions in initiating MPS development. The depolymerisation of F-actin inhibits MPS development in early axons (Xu *et al.*, 2013; Zhong *et al.*, 2014) and destabilises mature MPS (Qu *et al.*, 2017; Unsain *et al.*, 2018). However, what functions are subserved by F-actin in MPS initiation is unclear. Similarly, while microtubule integrity appears to be necessary for MPS maintenance (Zhong *et al.*, 2014; Qu *et al.*, 2017), its function in MPS development is unknown.

We present a chronological analysis of the βII-spectrin MPS development in embryonic DRG neurons using STED nanoscopy. Our findings reveal that βII-spectrin is recruited early to the axonal cortex and progressively matures to attain long-range periodic order and uniform spacing. In early stages, microtubule dynamics are essential for MPS formation but microtubules have a passive function in stabilising the mature MPS. We show that βII-spectrin is recruited to the axonal cortex via interactions with subplasmalemmal F-actin and the early MPS is dependent on actively nucleating actin networks. However, the mature, stable MPS is insensitive to the inhibition of F-actin nucleation. Using βII-spectrin knockout cells, we demonstrate that the actin-binding and PH-domains of βII-spectrin are necessary for its recruitment to the axonal cortex.

MATERIALS AND METHODS

Primary neuronal cultures

All experimental procedures were conducted in accordance with guidelines approved by the Institutional Animal Ethics Committee of the Indian Institute of Science Education and Research (IISER) Pune, India. Fertilized White Leghorn chicken eggs were obtained from Venkateshwara Hatchery Private Limited (Pune, India) and were incubated at 37 °C in a humidified incubator for 8-9 days.

Dorsal root ganglia (DRG) were isolated from embryos using sterile Leibovitz's L-15 medium (Hi-Media, AL204A) for dissection. Dissections were performed a laminar flow hood. Around 12-16 DRGs were isolated per embryo in the L-15 medium. The suspension was centrifuged at 3000 rpm for 3 min and the supernatant was removed. The DRGs in the pellet were resuspended in trypsin solution and incubated for 30 min at 37 °C. This was followed by a 3-minute spin at 3000 rpm to remove most of the trypsin solution and an L-15 wash to remove any remaining trypsin. The dissociated neurons were then plated onto glass coverslips or Poly-D-lysine-coated (0.1 mg/mL PDL; Merck, A-003-E) glass-bottom dishes. Neurons were cultured in serum-free medium composed of L-15 supplemented with 6 mg/mL glucose, 1× GlutaMAX (Gibco, 35050061), 1× B27 supplement (Invitrogen, A1895601), 50 ng/mL nerve growth factor (Gibco, 13290010), 0.006 g/ml methyl cellulose (34516, ColorconID), and 1× PenStrep (HiMedia, A001A). Cultures were maintained in a non-CO2 incubator at 37 °C.

Drug treatment of neurons

The specific drugs utilized, along with their corresponding treatment conditions, are described in table below. All the cultures were fixed and processed for immunofluorescence analysis at varied time-points. All drugs were prepared in dimethyl sulfoxide (DMSO) and DMSO-treated cultures served as vehicle controls for each drug treatment.

Drug	Source	Type of treatment	Time of addition	Concentration	Duration
Taxol	Santa Cruz (sc-201439)	Acute	DIV 1,2 & 4	10 μM	30 min
Nocodazole	Tocris Bioscience (2792)	Acute	DIV 1,2 & 4	10 μM	30 min
Latrunculin-A	Sigma Aldrich (L5163)	Acute	DIV 1,2 & 4	5 μM	15 min
Jasplakinolide	Tocris Bioscience (1228)	Acute	DIV 1,2 & 4	5 μM	30 min
Taxol	Santa Cruz (sc-201439)	Chronic	16 hrs post seeding	1 nM	Till DIV 2 & 4
Nocodazole	Tocris Bioscience (2792)	Chronic	16 hrs post seeding	10 nM	Till DIV 2 & 4
CK666	Merck (182515)	Acute	DIV 2,4 & 6	20 μM	30 min

SMIFH2	Merck (344092)	Acute	DIV 2,4 & 6	20 μM	30 min

Cell fixation and immunostaining for fluorescence imaging

Cultured neurons were fixed in 4% (w/v) paraformaldehyde (PFA) in phosphate-buffered saline (PBS) for 10 min at room temperature (RT). PFA was removed by washing with PBS, and the cells were then permeabilized with 0.1% (v/v) Triton X-100 in PBS for 5 min at RT, followed by blocking in 3% (w/v) bovine serum albumin (BSA) in PBS for 1 hr at RT. The cells were then incubated with the primary antibodies – (βII-spectrin 1:700 (BD bioscience; 612563), Anti-GFP 1:500 (Invitrogen; A11122) and βIII-tubulin 1:1000 (Santa-Cruz; sc-80005)) - overnight at 4 °C. The primary antibodies were removed the following day followed by 3x PBS washes, and the cells were incubated with the secondary antibodies – Alexa 488 conjugated anti-mouse or anti-rabbit (Invitrogen; A-11001, A-11008, respectively) – at 1:1000 dilution in blocking buffer for 1 h at RT. For super-resolution microscopy, neurons at different stages of *in vitro* culture (days in vitro or DIV) were mounted in a mixture of 10% Mowiol 4–88 in poly (vinyl alcohol) (Sigma-Aldrich, 81381) and 2.5% (w/v) DABCO (1,4-diazabicyclo [2.2.2] octane; Sigma-Aldrich, D27802). The mounted samples were stored overnight in the dark at 4 °C before imaging.

Plasmids construction and transfection

Human βII-Spectrin (from Addgene plasmid 31070: βII-Spectrin-HA) was incorporated into a pCAG-GFP containing vector by PCR. For the actin-binding deletion mutant (pCAG-ΔABD-βII-Spectrin-GFP) initial 3-277 aa was deleted from the pCAG-βII-Spectrin-GFP construct by PCR. Plasma membrane binding mutant (pCAG-βII-Spectrin-K2207Q-GFP) and Ankyrin binding mutant (pCAG-βII-Spectrin-Y187A-GFP) were created by introducing point mutations in pCAG-βII-Spectrin-GFP construct by PCR. Cells were suspended in Optimem® (Gibco) medium with 15-20 μg of plasmid. Subsequently, the cell suspension was electroporated using Super Electroporator NEPA21 Type II machine. The following parameters were used in all experiments: Poring pulse: 2x of 5 msec 125 V pulses with pulse interval of 50 msec and decay rate of 10%; polarity +. Transfer pulse: 5x of 50 msec 20 V pulses with pulse interval of 50 msec and decay rate of 40%; polarity +/-. After electroporation, the cells were seeded in glass-bottom dishes and incubated at 37 °C for relevant periods.

βII-Spectrin intensity analysis

Axons from DIV 1, 2, and 4 were stained for βII-Spectrin and imaged using confocal microscopy with 20x, 0.4NA objective. The middle region of the axon was selected and processed with ImageJ software for Otsu-based thresholding. A particle analyzer tool was used to estimate the integrated density and area of the axon, followed by CTCF calculation.

Fluorescence recovery after photobleaching & analysis

Primary neurons and differentiated βII-Spectrin KO SH-SY5Y cells were transfected via electroporation and used in experiments at various time points, ranging from 24 to 144 hr post-transfection. The following plasmids were used for transfection: pCAG-βII-Spectrin-GFP, pCAG-βII-Spectrin-K2207Q-GFP, pCAG-βII-Spectrin-Y187A-GFP, and pCAG-ΔABD-βII-spectrin-GFP.

Fluorescence recovery after photobleaching (FRAP) experiments were conducted using a Zeiss LSM 710 confocal microscope equipped with a 488 nm Argon laser for bleaching and a 37 °C humidified stage. Time-lapse images of GFP fluorescence were acquired at 2-second intervals using a Zeiss Plan-Apochromatic 63x/1.4 Oil objective with 3× optical zoom. Regions of interest (ROI) measuring maximum of ~2 × 1 microns (height × width) along the middle of the axon were iteratively photo-bleached (50-100 iterations) by scanning with a 488 nm laser at 100% power and a scanning speed of 6 μs/pixel. Post-bleach images were acquired with 15–30% laser intensity for 150 frames (2 second interval). The resulting images were analyzed using the ImageJ software.

For each region of interest (ROI), background fluorescence was subtracted at each time point. A reference region was used to correct for fluorescence loss due to bleaching during image acquisition by normalizing it to the pre-bleaching intensity. The background-corrected and acquisition-loss-corrected ROI intensities were then further normalized by setting the pre-bleaching intensity to 100% and the immediate post-bleaching intensity to 0%. The recovery curve was fitted to a single-phase association function from data plotted with 2s or 10s interval. The extra sum-of-squares F-test was used to compare plateau of curves. The half-life ($t_{½}$) was estimated from the fitted curve of individual axons and the % mobile fraction was calculated by averaging the last 5 frames of the recovering curve.

SH-SY5Y Neuroblastoma cell differentiation and culture

SH-SY5Y cells were grown and maintained in 60 mm Petri dishes in standard culture medium (DMEM/F12 supplemented with 10% fetal bovine serum [FBS] and 1% penicillin-streptomycin) at 37 °C in a 5% CO2 atmosphere. Cells were passaged upon reaching 80–90% confluence using trypsin-EDTA, and all experiments were conducted using cells with a passage number below 20. SH-SY5Y cells were differentiated into neuron-like cells over 12-14 days of Retinoic acid (RA) and Brain-derived neurotrophic factor (BDNF) treatment. Briefly, cells were seeded in a surface-coated 60 mm flask and treated with retinoic acid in DMEM/F12 supplemented with 1% FBS for 5 days, followed by 8 days of brain-derived neurotrophic factor (BDNF) treatment in serum-free medium.

For FRAP and STED microscopy, cells were trypsinized, transfected with the appropriate plasmids, and then reseeded on glass-bottomed, surface-treated dishes after RA treatment. They were maintained in serum-free BDNF-supplemented media for 6 days, and experiments were performed.

CRISPR/CAS9-mediated gene editing

Using an online CRISPR design tool (Ran *et al.*, 2013), two pairs of oligo DNAs encoding gRNAs were designed to target βII-Spectrin exon 16 sequences (gRNA 1: 5′**CCAGACAGCGATCGCCTCGGAGG**3′ and gRNA 2: 5′ **GAACGAGATCGACAACTACGAGG 3**′. These oligos were synthesized, annealed, and inserted into the BbsI site of the pSpCas9(BB)-2A-GFP (PX458) plasmid (Addgene plasmid no.48138). The resulting plasmids were amplified and introduced into SH-SY5Y cells via electroporation. GFP-positive cells were isolated through cell sorting. Western blot analysis was used to initially identify stably transfected clonal lines exhibiting complete depletion of SH-SY5Y expression.

Indel analysis of βII-Spectrin knockout cell lines

To examine indel mutations in SH-SY5Y βII-Spectrin knockout cells, genomic DNA was extracted from the knockout clonal lines. Subsequently, PCR amplification of exon 16 was performed using the extracted genomic DNA as a template. The following oligonucleotides were used as primers: forward 5′ CCCTGAAAAACCGAGAGGCC 3′ and reverse 5′ GCTCGTTCCATCCAGTGTCC 3′. The amplified DNA was then purified, and the resulting plasmids were sequenced to identify indel mutations.

STED imaging & analysis

STED imaging was conducted using a Leica TCS SP8 STED 3X microscope (Leica Microsystems) on chick dorsal root ganglion (DRG) neurons and differentiated SH-SY5Y neurons. Images were captured with an HC PL APO CS2 100x/1.4 STED WHITE oil immersion objective (Leica Microsystems) in both confocal and STED modes. Acquisition settings included 16x line averaging and detector gating on a Hybrid Detector (HyD, Leica Microsystems) with a range of 0.3 ns to 8 ns. The zoom factor was set to 6x, with a pixel size of up to 20 nm. A STED 592 depletion laser was used for all image acquisitions. All other settings were kept constant.

Images were deconvoluted using Huygens Professional software prior to analysis. Axonal regions were segmented into ~3 μm sections, and intensity versus distance profiles were generated for each segment. Autocorrelation functions using MATLAB (R2021a) were computed based on the intensity profiles of each segment. To obtain the average autocorrelation function, autocorrelation curves from all the selected axon segments were averaged for each experimental condition. The autocorrelation amplitude was defined as the difference between the first peak and the average of two adjacent valleys in the averaged autocorrelation curve. The average periodicity (or spacing) of the membrane periodic skeleton (MPS) structure for each ~3 μm segment was determined by the position of the first peak in the autocorrelation function. The diameter of each segment was calculated by measuring the edge-to-edge distance between spectrin signals.

Axonal ablation and analysis

DRG neurons were grown on a glass-bottom dish without any coating to obtain detached axons. Axons of DIV1, DIV2, and DIV4 neurons were subjected to laser ablation using a home-built laser ablation setup. This setup consists of a 355 nm, 25 mJ, 350 ps pulsed laser (PowerChip PNV-M02510-100; Teem Photonics, Meylan, France) coupled to the side port of a Leica TCS SP8 confocal microscope using a custom filter-cube and focussed on the sample using 40x/0.75 dry Phase Contrast objective. A custom-made 90° rotated filter cube having a UV-reflecting dichroic filter (T387lp-UF3, Chroma) was used to reflect the laser light into the objective. During and after ablation, phase contrast images were recorded using a CCD camera (Phantom VRI-MICRO-C210-16GB-M, Vision Research) at 2000 fps for 0.8 seconds to capture the initial fast retraction process of the ablated axons. A custom MATLAB code was employed to quantify the evolving gap distance. The x- and y-coordinates obtained were converted to distance values and plotted using GraphPad software. Estimation statistics (Ho *et al.*, 2019; Estimation Stats), Cohen's d and two-sided permutation test between the final gap length post-ablation was determined. The F-test was used to compare the plateaus of the evolving curve after fitting the data to a single-phase association model.

Statistical analysis

All statistical analyses and visual representations were conducted using GraphPad Prism 10 (10.4.0). In the figures, data are presented with a central line indicating the mean, along with error bars displaying the standard error of mean (SEM). The number of data points analyzed for each graph is indicated in the figure legends. Statistical test along with correction tests used for the analysis are mentioned in the figure legend.

RESULTS

Axonal βII-spectrin progressively develops a highly periodic organisation

To investigate the developmental trajectory of the-spectrin MPS in embryonic dorsal root ganglion (DRG) neurons, dissociated DRG neuron primary cultures were fixed at various time points, immunolabelled with βII-spectrin antibodies, and imaged using STED nanoscopy. We quantified the early development of the MPS by imaging the central regions of axons cultured for 1, 2, 4, and 6 days *in vitro* (DIV), using autocorrelation analysis of the βII-spectrin signal (Fig 1A,B). We quantified the degree of periodicity (autocorrelation amplitude at the first peak) and the periodic spacing of the βII-spectrin rings (periodicity) from the autocorrelation curves (Fig. 1C,D). The representative micrographs (Fig. 1A) depict the emergence and evolution of the periodic organisation of βII-spectrin in the axons across development. βII-spectrin was already localised to the axonal shaft by DIV1 but its organisation was weakly periodic (Fig. 1A). However, the average autocorrelation amplitudes increased progressively with DIV (Fig. 1B,C), indicating the consolidation of long-range periodic order. Concomitant with the increase in the extent of periodicity, the spacing (periodicity) of the βII-spectrin signal (Fig. 1D) reduced with the age of the cultured neurons from 214 ± 6.17 nm in DIV1 to 196.7 ± 2.52 nm in DIV2. It further decreased to 192.9 ± 8.9 nm and 185.8 ± 4.3 nm on DIV 4 and DIV6, respectively. The developmental maturation of the MPS was further revealed by the progressive reduction of the coefficient of variation of the βII-spectrin spacing (Fig. 1D), decreasing from 25.9 at DIV1 to 4.3 at DIV6. The high variability of the periodicities during the early stages was expectedly associated with lower autocorrelation amplitudes (Fig. 1E). The autocorrelation amplitude increased with development as the spacing converged to 185.8 ± 4.3 nm by DIV 6. Interestingly, in these axonal segments, the amount of βII-spectrin per unit area is unchanged across DIV1, 2 and 4 (Fig. S1A), though the distribution becomes highly periodic. This suggests MPS maturation is dominated by the re-organisation of spectrin, recruited to the cortex early in development, from a relatively disordered to an ordered periodic scaffold.

To evaluate whether MPS maturation across these early developmental stages influenced the axonal morphology, we measured the diameter of the βII-spectrin rings as a surrogate measure of axonal diameter. MPS maturation across DIVs correlated with a reduction in diameter (Fig.1F). This observation is consistent with the role of the MPS in regulating the axonal diameter (Costa *et al.*, 2020; Wang *et al.*, 2020) and suggests progressive constriction of the axonal shaft as the MPS matures. Interestingly, the decrease in diameter was already substantial by DIV2. This observation, together with a significant increase in autocorrelation amplitude (Fig. 1B) in DIV2 (compared to DIV1) suggests an early maturation of the βII-spectrin MPS in DRG neurons.

The axon is contractile (Mutalik *et al.*, 2018) and the MPS has been associated with axonal tension and pre-stress (Krieg *et al.*, 2014; Dubey *et al.*, 2020). To assess if early MPS maturation contributes to axonal tension, we employed laser-induced axonal ablation of DIV1, 2 and 4 neurons (Fig. S1B) and followed the evolution of the gap distance between the two ends following ablation. The rate of change of the gap distance may depend on passive stresses, active contractility or progressive cytoskeletal remodelling. However, the early, exponential response is likely to be dominated by axonal pre-tension. F-test comparing the plateaus of the one-phase association fits revealed that DIV4 axons exhibit greater pre-stress than DIV1 and

DIV2 axons (Fig. 1G), while the quantitative analysis of gap distance at 0.74 seconds revealed a substantial effect size (Cohen's d=0.93; p=0.0078) compared to DIV1 (Figs. 1G, S1C). Maturation of the βII-spectrin MPS thus appears to correlate with the evolution of axonal tension. However, the change observed is modest and there is substantial pre-tension at DIV1 when the βII-spectrin MPS is only weakly periodic.

Collectively, these data reveal the maturation kinetics of the βII-spectrin MPS in DRG axons in early development. βII-spectrin is recruited early to the axonal cortex followed by progressive establishment of periodic order, which is concomitant with decreasing in axonal diameter and increasing in axonal pre-stress.

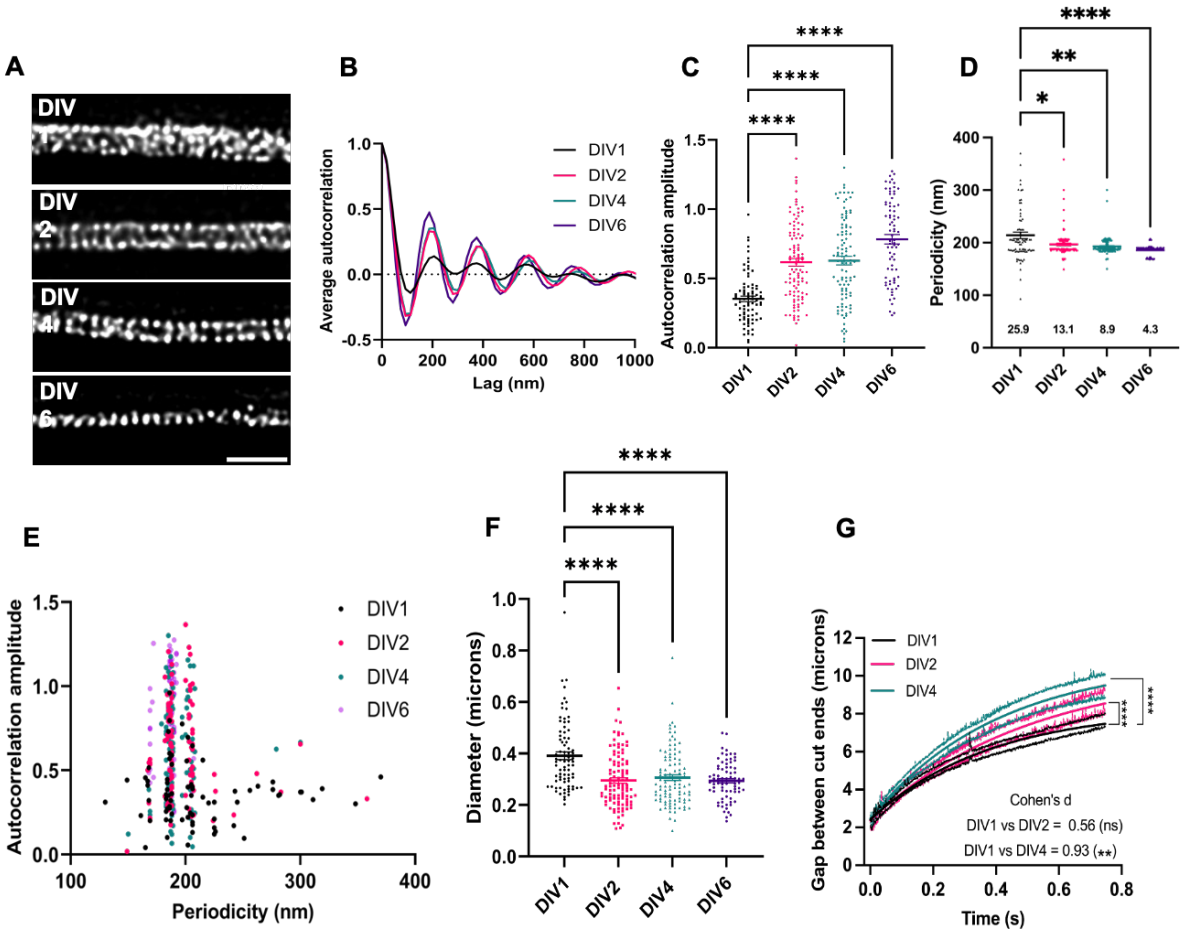

Figure 1: The βII-spectrin membrane periodic skeleton (MPS) assembles progressively. (A) Representative micrographs of single optical sections from STED nanoscopy of DIV1, DIV2, DIV4, and DIV6 DRG axons stained with βII-spectrin antibody. Scale bar: 1 μm. (B) Average autocorrelation curves across multiple axonal regions. (C) The autocorrelation amplitudes of the βII-spectrin rings. Amplitudes were quantified as the difference between the first peak and the average of the first two valleys of the autocorrelation curve. The data were analysed using the Brown-Forsythe and Welch ANOVA test with multiple comparisons corrected by Games -Howell's test.(D) Periodicity across DIVs demonstrates a reduction in the spacing between the βII-spectrin rings. The data were analysed using the Brown-Forsythe and Welch ANOVA test with multiple comparisons corrected by Games -Howell's test. The numbers below each data set indicate the coefficient of variation of the distribution. (E) Plot of the autocorrelation amplitudes against periodicity for all DIVs, indicating the degree of autocorrelation and the relative distribution of MPS periodicity. (F) βII-spectrin ring diameter across DIVs. The data were analysed using the Kruskal-Wallis test with multiple comparison corrected by Dunn's test. For A-F, 80-100 axonal segments from 3 biological replicates for each DIV were analysed. (G) The evolving gap length between cut ends following ablation is represented as a one-phase fit of the means (± SEM). Curve fits were compared using the extra sum-of-squares F-test. The

effect sizes and significance, represented by Cohen's d and two-sided t-test, obtained by comparing the gap length in the last 10 frames (till 0.74 sec) using Estimation statistics (Fig S1C) are indicated. The data are derived from n=19 (DIV1), n=15 (DIV2) and n=16 (DIV4) axons from at least three biological replicates. (ns, $p > 0.05$; *, $p \leq 0.05$; **, $p \leq 0.01$; ****, $p \leq 0.0001$).

F-actin and microtubules are required for βII-spectrin MPS development

Several studies have implicated both the actin and microtubule cytoskeletal systems in the maintenance of the F-actin/βII-spectrin MPS, with most focussing on late-stage neurons. We evaluated the role of axonal F-actin and microtubules in the early development of the βII-spectrin MPS. DRG neurons at DIV1, 2, and 4 were acutely exposed to drugs that destabilised or stabilised the two cytoskeletal systems before fixation and evaluation of the βII-spectrin MPS via STED nanoscopy.

Suppression of F-actin polymerisation by latrunculin-A (Lat-A; 5 μM, 15 min) or microtubules polymerisation by nocodazole (Noco; 10 μM, 30 min) disrupted the autocorrelation curves and reduced the autocorrelation amplitudes across all DIVs (Fig. 2A-B,D-E,G-H). Furthermore, periodicity analysis revealed an increased coefficient of variation of the MPS spacing upon depolymerisation of the actin or microtubule cytoskeletons (Fig. 2C,F,I).

Acute treatment with the F-actin stabilising jasplakinolide (Jasp; 5 μM, 30 min) or microtubule stabilising paclitaxel (Taxol; 10 μM, 30 min), however, did not affect the autocorrelation or average autocorrelation amplitudes at any of the DIVs (Fig. 2A-B,D-E,G-H). While the periodicity analysis revealed no difference in the mean βII-spectrin spacing, there was a notable decrease in the coefficient of variation of the spacing upon either actin or microtubule stabilization at DIV1 but it was not obvious at DIV2 and DIV4 when the MPS is already well organised (Fig. 2C,F,I). The latter result may suggest pharmacological stabilisation of labile F-actin and microtubules in early developmental stages facilitates the maturation of the βII-spectrin MPS. The lability of F-actin at early stages of MPS development has been previously suggested as periodic F-actin is not detectable in young axons though spectrin MPS is easily discernible (Zhong *et al.*, 2014).

These experiments demonstrate the requirement of both F-actin and microtubules in the development of the βII-spectrin MPS.

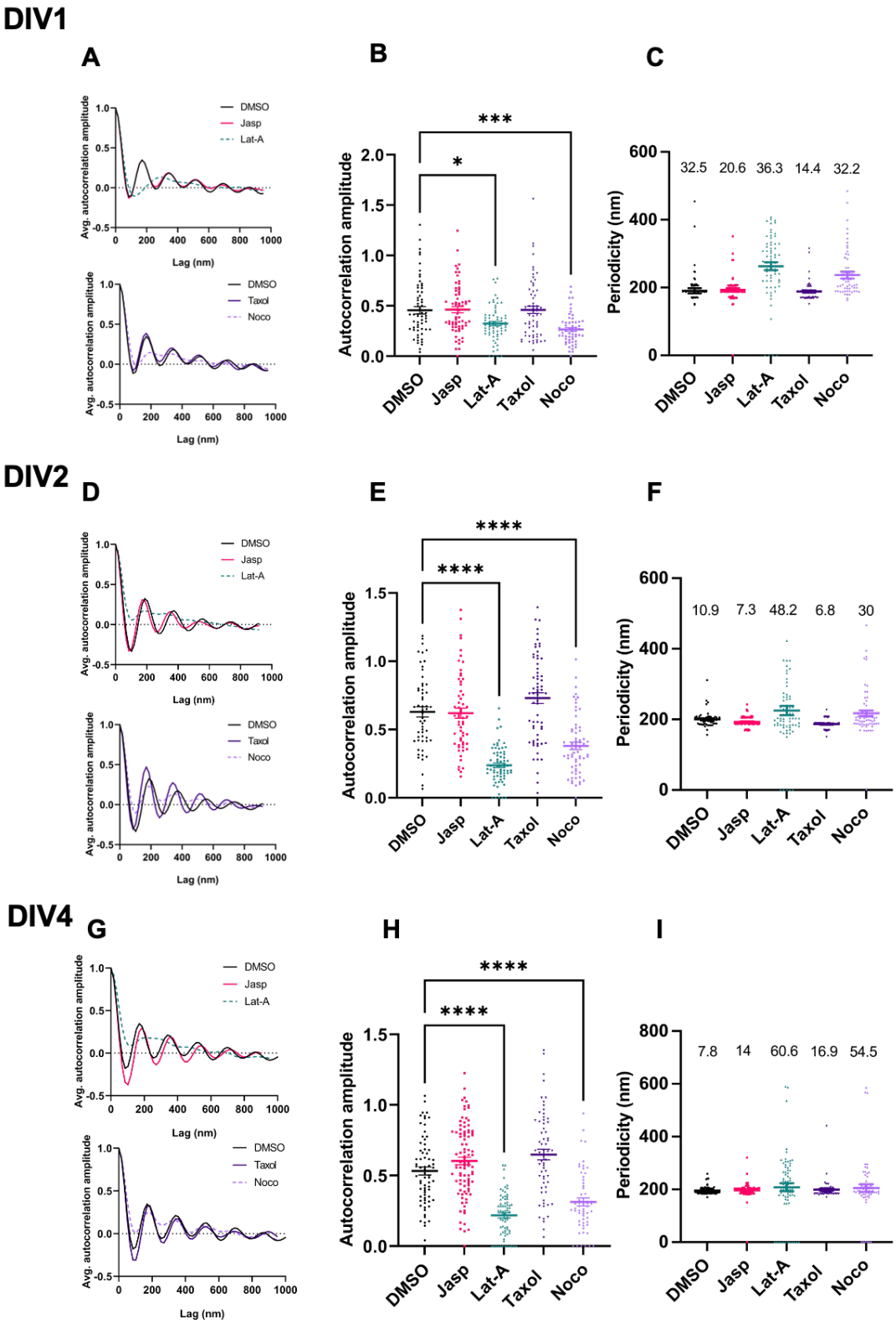

Figure 2: Destabilization of F-actin and microtubules affects MPS development and stability. (A,D,G) Average autocorrelation curves of axonal segments across DIVs treated with DMSO (control), Jasplakinolide (Jasp), latrunculin-A (Lat-A), Paclitaxel (Taxol) , and Nocodazole (Noco). (B,E,H) The autocorrelation amplitudes of the βII-spectrin rings across treatments and DIVs. The data were analysed using the Brown-Forsythe and Welch ANOVA test with multiple comparisons corrected by Games -Howell's test (ns, $p > 0.05$; *, $p \leq 0.05$; ***, $p \leq 0.001$; ****, $p \leq 0.0001$). (C,F,I) Periodicity (spacing) across DIVs treated with indicated drugs. The numbers below each data set indicate the

coefficient of variation of the distribution. The numbers above each data set indicate the coefficient of variation of the distribution. For A-I, 60-90 axonal segments from 3 biological replicates for each DIV were analysed.

Microtubule dynamics is necessary to initiate MPS development

The involvement of microtubules in destabilising the early βII-spectrin MPS (Fig. 2) led us to investigate if microtubule dynamics were required for the initiation and consolidation of MPS. We developed an early, chronic treatment protocol where a low dose of Noco (10 nM) or Taxol (1 nM) was added 16 h post-seeding (to allow for neuritogenesis) and the cultures fixed at DIV2 and DIV4 (Fig. 3A). Chronic disruption of microtubule polymerisation by Noco disrupted MPS formation at both DIV 2 and 4, as shown by the averaged autocorrelation curves and reduced autocorrelation amplitudes (Fig. 3B-D). Interestingly, in contrast with acute exposure to Taxol (Fig. 2), chronic stabilisation of microtubule by Taxol compromised MPS formation (Fig. 3B-D) at both DIV2 and 4. Both microtubule depolymerisation and stabilisation increased the coefficient of variation of the periodicity (Fig. 3E).

Chronic treatment of hippocampal neurons with taxol has previously been shown to induce multiple axon-like processes with MPS (Zhong *et al.*, 2014). However, this study was performed at later stages and the MPS of these axon-like processes were not quantitatively evaluated. Our data suggest that a balance of stable and dynamic microtubules is required to initiate MPS formation (Fig. 3), however, the maintenance of the relatively more established MPS is only sensitive to microtubule depolymerisation (Fig.2) but not stabilisation. Perhaps at later stages, microtubules have a more structural function in supporting the mature MPS.

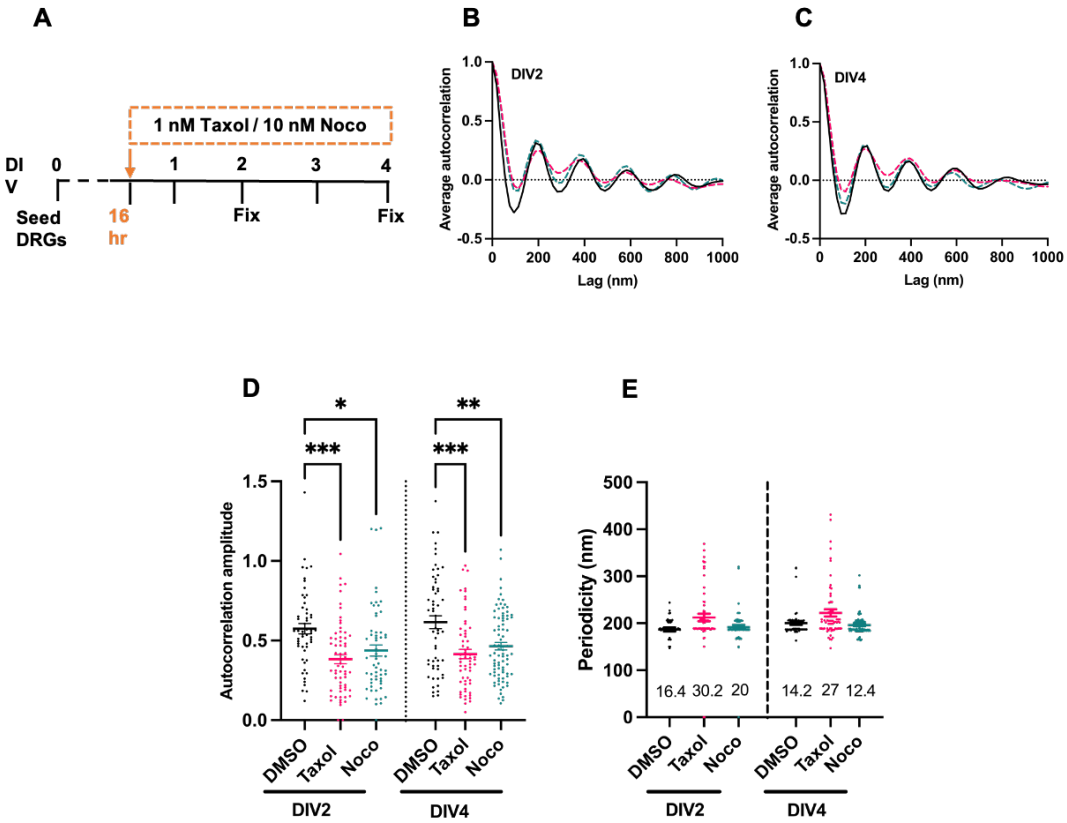

Figure 3: Microtubule dynamics is crucial for MPS formation. (A) Timeline of the experiment. 1 nM Taxol or 10 nM Nocodazole was added 16 hr after seeding the neurons and fixed either after

another 32 hrs (DIV2) or after 80 hrs (DIV4). (B,C) Average autocorrelation curves drop for βII-spectrin stained axons from cultures treated with 10 nM nocodazole (green dotted curve) and 1 nM Taxol (pink dotted curve) compared to DMSO (black curve) (D)The autocorrelation amplitudes of the βII-spectrin rings. The data were analysed using the Brown-Forsythe and Welch ANOVA test with multiple comparisons corrected by Games -Howell's test (*, $p \leq 0.05$; **, $p \leq 0.01$; ***, $p \leq 0.001$). (E) Periodicity across DIVs demonstrates an increase in variability between the βII-spectrin rings. The numbers below each data set indicate the coefficient of variation of the distribution. For B-E, 55-80 axonal segments from 3 biological replicates for each DIV were analysed.

Actin nucleators Arp2/3 and Formins regulate MPS development only in the early stages

F-actin structures in cells are initiated by the activity of actin nucleators, which also modulate the morphology and dynamics of these structures. Previous reports indicate that MPS formation is impaired in neurons derived from *Drosophila* carrying loss-of-function mutations in the actin nucleators Arp2/3 and the formin DAAM (Qu *et al.*, 2017). Given the dependence of the βII-spectrin MPS on F-actin (Fig. 2), we investigated the contribution of Arp2/3 and formins in MPS organisation at different developmental time points.

We exposed DRG neurons at different DIVs to the Arp2/3 complex inhibitor, CK666 (20 μM for 30 mins) or the formin inhibitor, SMIFH2 (20 μM for 30 mins). Inhibition of Arp2/3 or the formins in early-stage neurons (DIV2 and DIV4) led to the disorganisation of the βII-spectrin MPS with decreased autocorrelation and average autocorrelation amplitudes (Fig. 4A-C). These were accompanied by an increase in the variability of the MPS spacing though the mean values were not statistically different. However, at DIV 6, inhibition of neither the Arp2/3 complex nor formin activity disrupted the abundance or periodicity of the MPS. These results suggest that MPS development requires both the linear (formins) and branched nucleators (Arp2/3) at the early developmental stages, however, actin nucleation is dispensable for the maintenance of stable MPS.

The formin inhibitor, SMIFH2, also inhibits myosin II at high doses (Nishimura *et al.*, 2021). As inhibition of myosin II increases the axonal diameter (Costa *et al.*, 2020; Wang *et al.*, 2020), we tested if treatment with SMIFH2 altered axonal diameter at DIV6 (no effect on MPS organisation). No change in the diameter of the βII-spectrin ring was observed following SMIFH2 treatment (Fig S4) suggesting that the dose used in our experiments does not inhibit myosin II significantly.

F-actin is necessary to crosslink multiple spectrin heterotetramers to form the mature axially concatenated arrangement of alternating F-actin rings and spectrins. In addition, the recruitment and retention of spectrin heterotetramers to the axonal cortex, prior to the development of a strongly periodic scaffold, could depend on subplasmalemmal F-actin. Our data indicating the sensitivity of the earlier stages to the inhibition of F-actin nucleation suggest labile F-actin structures with faster F-actin turnover at these stages. However, at later stages (DIV6), F-actin structures are more stable with reduced dependency on fresh nucleation and/or filament elongation (formins can enhance both F-actin nucleation and barbed end polymerisation (REF)).

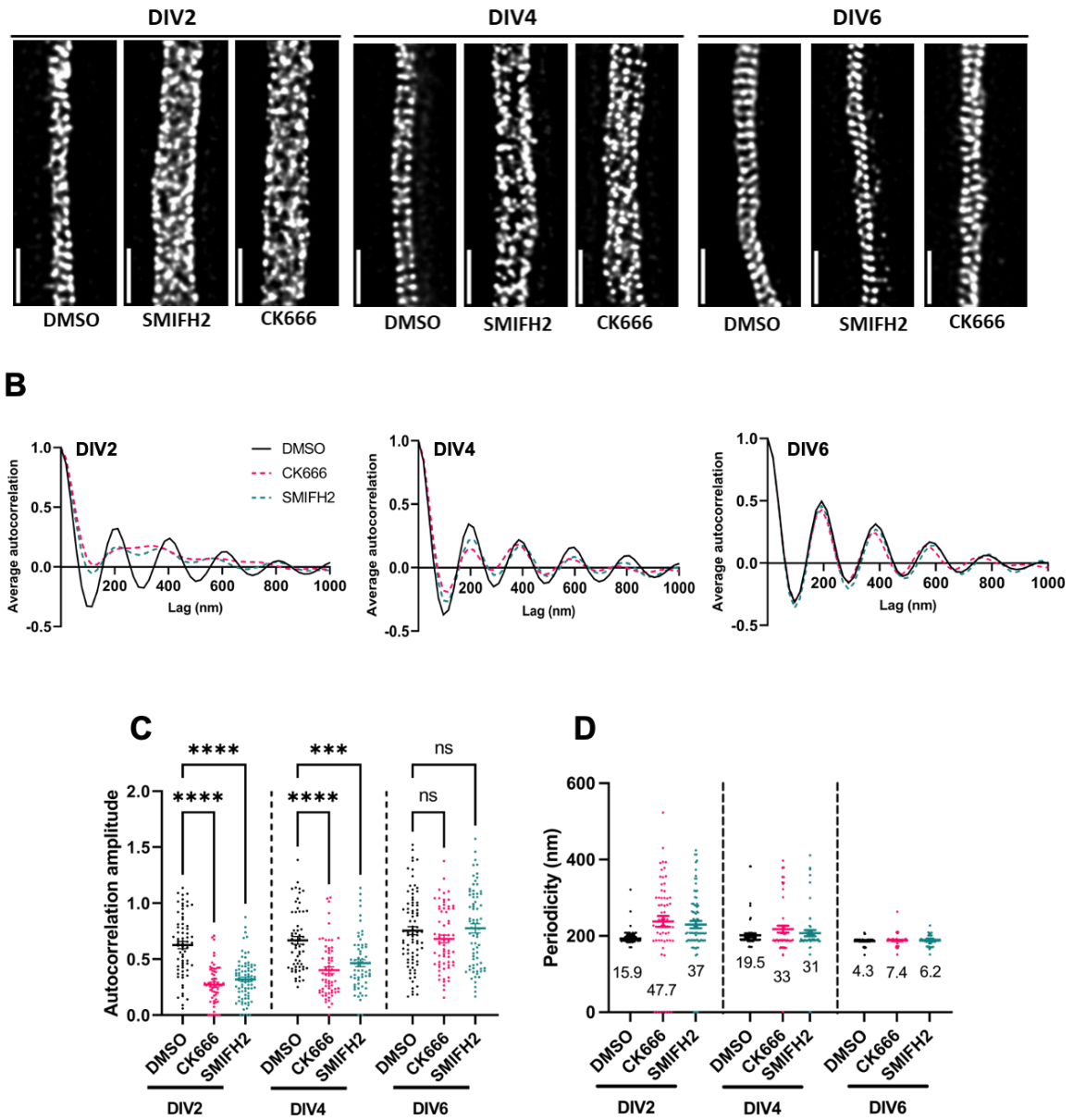

Figure 4: Formins and Arp2/3 affect MPS formation and maintenance. (A) Representative micrographs of single optical sections from STED nanoscopy of DIV2, DIV4, and DIV6 DRG axons stained with βII-spectrin post-treatment with DMSO control, Formin inhibitor; (SMIFH2; 20 μM, 30 min) or Arp2/3 inhibitor (CK666; 20 μM, 30 min). Scale bar: 1 μm (B) Average autocorrelation curves across multiple axonal regions for all treatments. (C) The autocorrelation amplitudes of the βII-spectrin rings. The data were analysed using the Brown-Forsythe and Welch ANOVA test with multiple comparisons corrected by Games -Howell's test (ns, $p > 0.05$; ***, $p \leq 0.001$, ****, $p \leq 0.0001$) (D) Periodicity across DIVs demonstrates an increase in variability between the βII-spectrin rings at DIV2 and 4. The numbers below each data set indicate the coefficient of variation of the distribution. For B-D, 60-70 axonal segments from 3 biological replicates for each DIV were analysed.

βII-spectrin progressively associates with the axonal cortex via interactions with F-actin

As the axon develops, βII-spectrin is recruited to the cellular cortex and progressively evolves into a highly periodic organisation (Fig. 1). We find early subplasmalemmal recruitment of βII-spectrin by DIV1 (Fig. 1A-D) and a dependence

F-actin (Figs. 2 and 4) in initiating MPS formation. To evaluate the dynamics of subplasmalemmal βII-spectrin, we employed fluorescence recovery after photobleaching (FRAP) analysis of DRG neurons transfected with GFP-tagged βII spectrin (βII-spectrin-GFP) at different developmental stages (Fig. 5A). To exclude cytoplasmic spectrin resulting from overexpression, only axons with low expression of βII spectrin-GFP were selected for the analysis.

Analysis of the normalized recovery curves and the mobile fraction, demonstrated a gradual decrease in the overall mobility of βII-spectrin, with a marked reduction as development progresses from DIV1 to DIV4 (Fig. 5B,C). The half-life ($t_{1/2}$) of the recovery was similar across DIVs indicating no change in the rate of diffusion of βII-spectrin (Fig. S5A). These data are consistent with the increase in the autocorrelation amplitude from DIV1 to DIV4 (Fig. 1), indicating that the βII-spectrin scaffold becomes increasingly stable with development. However, even at the early stages (DIV1), the mobile fraction is under 50%. This suggests that βII-spectrin is already recruited to the axonal cortex by DIV1 with restricted mobility.

Recruitment of spectrin heterotetramers to the cortex may involve interactions with the cortical F-actin. The sensitivity to F-actin deregulation observed earlier (Figs. 2 and 4) likely reflects this association. To explore the role of F-actin in βII-spectrin mobility, we treated βII-spectrin-GFP transfected DIV1, 2, and 4 DRG neurons with 5 μM Lat-A for 15 min (same dose as that used in data represented in Fig. 2) before FRAP analysis. In contrast to the DMSO-treated control recovery curves for DIV1 and DIV2 neurons, the Lat-A-treated axons exhibited increased βII-spectrin mobility with an elevated mobile fraction (Fig. 5D-E). However, the recovery kinetics of βII-spectrin-GFP in DIV4 axons treated with Lat-A were comparable to the DMSO-treated controls. In all cases, there was no change in the $t_{1/2}$ of the recovery (Fig. S5 B).

These data suggest that a significant proportion of βII-spectrin is associated with the axonal cortex as early as DIV1 and constitutes a stable spectrin pool. A major component of this early association is via interactions with subplasmalemmal F-actin though this dependence is reduced by DIV 4, perhaps due to the recruitment of other interactions that stabilise the association or increased resistance of mature cortical F-actin to depolymerisation. The increased stability of βII-spectrin correlates with the progressive establishment of long-range, periodic order of the MPS with developmental time (Fig. 1).

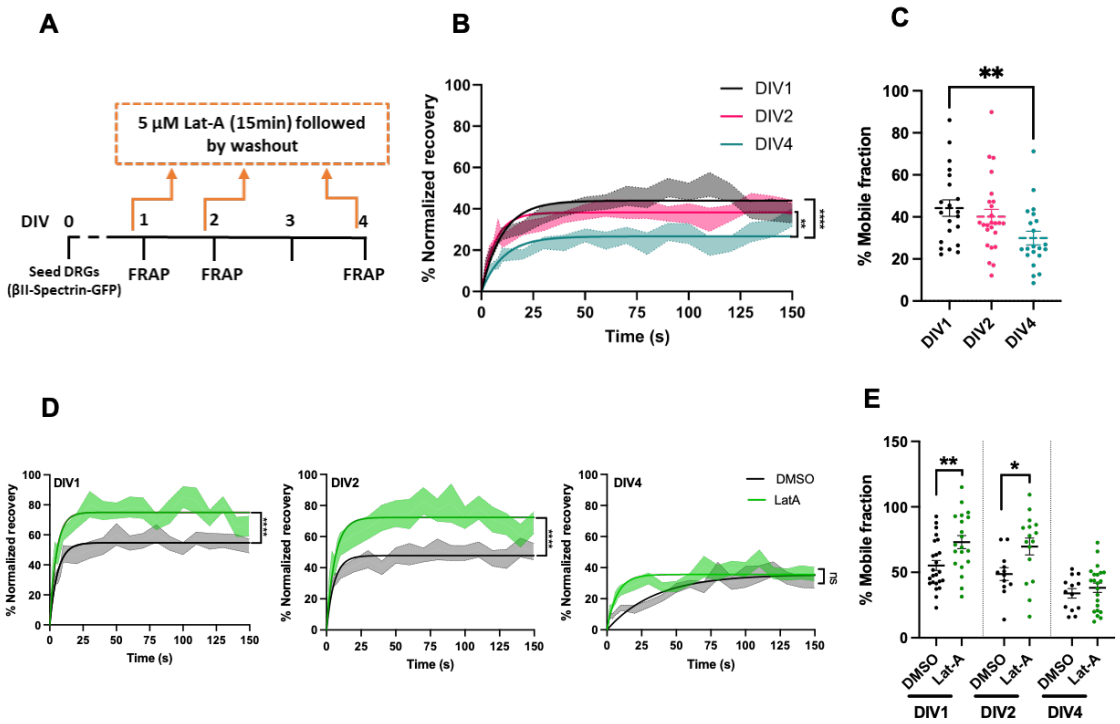

Figure 5: Spectrin mobility is correlated with MPS maturation and dependent on F-actin mediated cortical recruitment. (A) Timeline of the experiments. DRGs were transfected with βII-spectrin-GFP during seeding. FRAP experiment was conducted at DIV1, DIV2, and DIV4. For actin destabilization, Latrunculin A (Lat-A; 5 µM, 15 min) was administered for 15 mins before FRAP analysis. (B) βII-spectrin-GFP FRAP recovery curves for the DIV1, DIV2, and DIV4 axons. The recovery curves are represented as a one-phase fit of the means (± SEM). Plateau of curves were compared using the extra sum-of-squares F-test (C) Quantification of the % mobile fraction. The data were analysed using the Mann-Whitney test. For A-C, 16-30 neurons for all DIVs from 3 biological replicates were analysed (D) βII-spectrin-GFP FRAP recovery curves for DRG axons treated with Lat-A across DIV1 DIV2 and DIV4. The green and black traces represent the average one-phase fit for Lat-A- and DMSO-treated neurons, respectively. The recovery curves are represented as a one-phase fit of the means (± SEM). Plateau of curves were compared using the extra sum-of-squares F-test (E) Quantification of the % mobile fraction. The data were analysed using the Mann-Whitney test. In this experiment, 12-24 neurons for all DIVs from 3 biological replicates were analysed. ns, $p > 0.05$; **, $p \leq 0.01$; ****, $p \leq 0.0001$.

F-actin and membrane interactions recruit βII spectrin to the axonal cortex for MPS development

βII-spectrin is recruited to and stably associates with the axonal cortex early in development (Fig. 5). To examine how early recruitment influences MPS development and dissect the underlying mechanisms we developed differentiated SH-SY5Y human neuroblastoma cells as a model. Using a differentiation protocol (see Methods) involving sequential treatment with retinoic acid (RA) and brain-derived neurotrophic factor (BDNF), we characterised the development of the βII-spectrin MPS in the axon-like SH-SY5Y neurites (Fig. 6A). βII-spectrin autocorrelation and the autocorrelation amplitude both increased following BDNF treatment for 4, 6 and 8 days (Fig. 6B-D). The periodicity measurements demonstrated a progressive decrease in the MPS spacing variability reaching 191 ± 3.17 nm after 8 days (Fig. 6E), indicating a developmental pattern comparable to DRG neurons (Fig. 1). Next, we generated βII-Spectrin knockout SH-SY5Y cells (βII-Spectrin KO) using CRISPR-Cas9 technology and verified the knockout through

genomic sequencing (Fig. S6 A,B) and immunoblotting (Fig. 6 F). As expected, the βII-Spectrin-KO SH-SY5Y neurons displayed reduced axonal lengths (Fig. S6C,D), consistent with the phenotype reported for neurons derived from βII-Spectrin knockout mice (Lorenzo *et al.*, 2019).

To parse the contributions from various βII-spectrin interactions, we generated variants of βII-spectrin fused with a green fluorescent protein (GFP) tag (Fig. 7A). These included the full-length human βII-Spectrin protein, as well as mutants lacking ankyrin B binding (βII-Spectrin-Y1874A), plasma membrane recruitment via the PH domain (βII-Spectrin-K2207Q), and actin-binding (βII-Spectrin-ΔABD). We imaged GFP-labelled axons using STED nanoscopy 6 days after the transfection of these constructs in the βII-Spectrin knockout SH-SY5Y cells (Fig. 7A). The full-length βII-spectrin and ankyrin B binding deficient protein (βII-Spectrin-Y1874A) were recruited to the axonal cortex and formed a periodic scaffold (Fig. 7B-D). However, both the PH domain (βII-Spectrin-K2207Q) and actin-binding domain (βII-Spectrin-ΔABD) mutants were unable to form a periodic MPS structure, as quantified by the average autocorrelation curves and autocorrelation amplitudes (Fig. 7B-D). Additionally, periodicity analysis showed a higher coefficient of variation for both these mutants compared to the full-length control (Fig. 7E). These findings are in agreement with findings from mouse βII-Spectrin (Zhou *et al.*, 2022) and demonstrate βII-spectrin recruitment to the subplasmalemmal cortex via actin-binding and membrane interactions of the PH-domain to form the MPS.

To investigate the subplasmalemmal recruitment of βII-spectrin further, we performed FRAP analysis of βII-Spectrin KO cells following transfection with different βII-Spectrin mutants. The recovery kinetics of ankyrin B -binding deficient protein (βII-Spectrin-Y1874A) was comparable to the full-length protein (Fig. 8A,B). However, βII-Spectrin deficient in F-actin binding (βII-Spectrin-ΔABD) had a significantly higher mobile fraction and reduced $t_{1/2}$ indicating compromised recruitment to the axonal cortex (Fig. 8A,B). This observation is consistent with the elevated mobile fraction of βII-Spectrin observed upon F-actin disruption by Lat-A treatment in primary DRG neurons (Fig. 5D,E).

The mobile fraction estimated from the recovery curves of the PH domain mutant (βII-Spectrin-K2207Q) was comparable to the wild-type protein (Fig. 8A,B). However, the $t_{1/2}$ of the recovery was significantly reduced (Fig. 8C). This suggests no change in the proportion of bound βII-Spectrin-K2207Q molecules but a higher diffusion rate. Given that transfection of βII-Spectrin-K2207Q results in compromised recovery of the MPS (Fig. 7 B-E), this implicates βII-Spectrin PH domain interactions in constraining the kinetics of βII-Spectrin and, in turn, its recruitment to the cortical scaffold.

Collectively, these data identify βII-Spectrin interactions with F-actin and the plasma membrane for early recruitment and stabilisation of βII-Spectrin at the axonal cortex as a necessary prerequisite for MPS development.

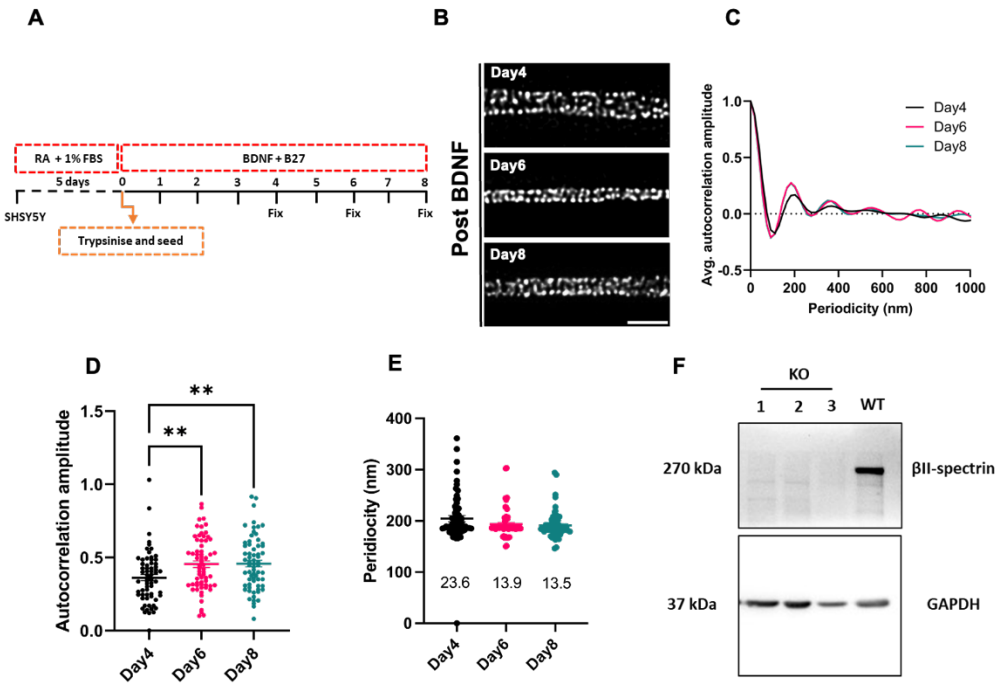

Figure 6: MPS in differentiated SH-SY5Y neurons. (A) Timeline indicating the differentiation protocol of SH-SY5Y cells. (B) Representative micrographs of single optical sections from STED nanoscopy of βII-spectrin stained differentiating neurons (4, 6, and 8 days post-BDNF). Scale bar: 1 µm. (C, D) Average autocorrelation curves and quantification of autocorrelation amplitudes across time points. The data were analyzed using the Brown-Forsythe and Welch ANOVA test with multiple comparisons corrected by Games -Howell's test. (**, $p \leq 0.01$). (E) Periodicity across days demonstrates a reduction in variability. The numbers below each data set indicate the coefficient of variation of the distribution. For B-E, 65 axonal segments from 3 biological replicates for each time-point were analysed. (F) Immunoblot validating the CRISPR-Cas9-based generation of βII-spectrin knockout line in SH-SY5Y cells (βII-Spectrin KO). KO-1 was used for all subsequent analyses.

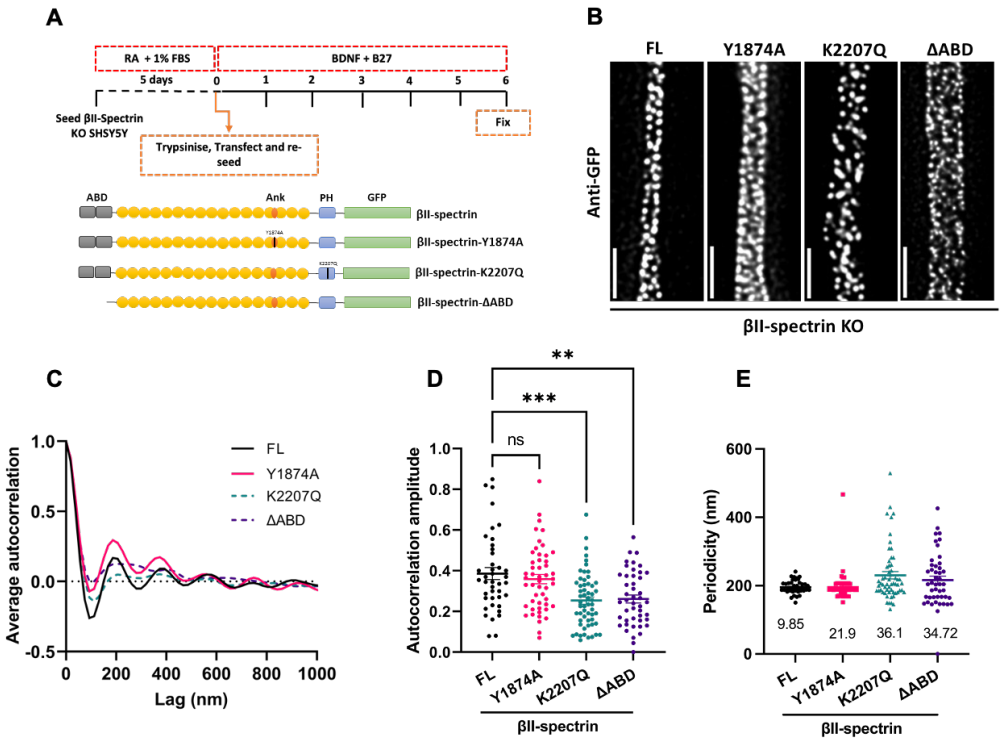

Figure 7: Actin-binding and plasma membrane interactions of βII-spectrin are necessary for MPS development. (A) Timeline indicating the differentiation protocol of βII-Spectrin KO cells and experimental procedures. βII-spectrin KO were transfected mid-differentiation with βII-spectrin variants indicated. The domains are denoted as follows: GFP-tag in green, actin-binding domain (ABD) in grey, ankyrin domain-binding domain in orange, and plasma membrane-binding domain in blue. (B)) Representative micrographs of single optical sections from STED nanoscopy of anti-GFP stained differentiated neurites (day 6 post-BDNF) transfected with βII-spectrin variants.(C) Average autocorrelation curves and quantification of autocorrelation amplitudes for all βII-spectrin variants. The data were analysed using the Brown-Forsythe and Welch ANOVA test with multiple comparisons corrected by Games -Howell's test (ns, $p > 0.05$; **, $p \leq 0.01$; ***, $p \leq 0.001$). (E) Periodicity demonstrates high variation in the spacing between the βII-spectrin rings in K227Q and ΔABD variants. The numbers below each data set indicate the coefficient of variation of the distribution. In this experiment, 40–60 axonal regions were examined for each condition across 3 biological replicates.

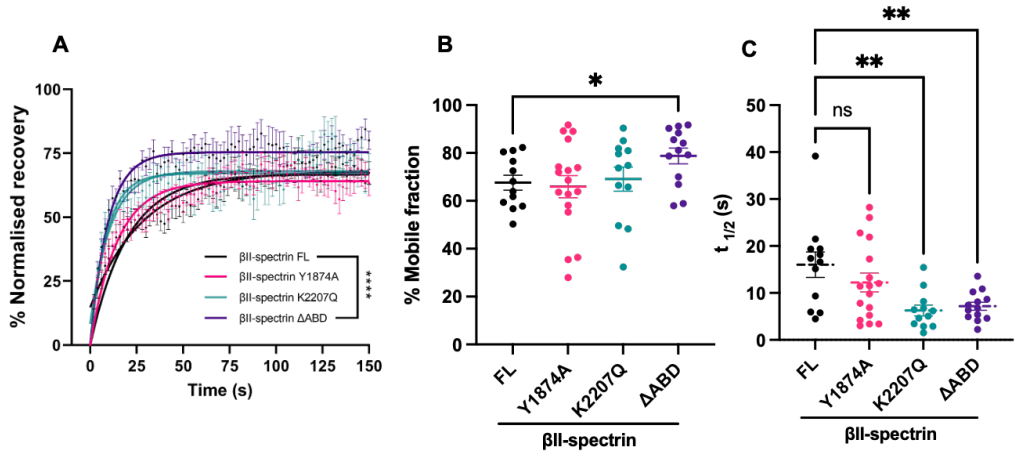

Figure 8: Actin-binding and membrane interactions drive βII-spectrin recruitment and mobility (A) FRAP recovery curves of mutant and βII-FL-spectrin expressing βII-Spectrin KO cells 6 days after transfection and BDNF treatment. The recovery curves are represented as a one-phase fit of the means (± SEM). Plateau of curves were compared using the extra sum-of-squares F-test (B) Quantification of the % mobile fraction. The data were analysed using the Mann-Whitney test.(C) $t_{1/2}$ values extracted from the fit were analysed using the one-way ANOVA test. In this experiment, 12-24 neurons for all DIVs from 3 biological replicates were analysed. ns, $p > 0.05$; *, $p \leq 0.05$; **, $p \leq 0.01$; ****, $p \leq 0.0001$.

DISCUSSION

Spectrin heterotetramer-based subplasmalemmal scaffolds are common across cell types(Ghisleni *et al.*, 2020; Leterrier and Pullarkat, 2022) but form a unique periodic structure with long-range order in neuronal axons. Given the myriad functions ascribed to the axonal MPS (Albrecht *et al.*, 2016; Lorenzo *et al.*, 2019; Zhou *et al.*, 2019, 2022; Costa *et al.*, 2020), there is considerable interest in understanding the early development of the axonal MPS. In this study, we focus on embryonic DRG neurons to uncover the cytoskeleton-mediated mechanisms underlying the recruitment of spectrin to the axonal cortex, the maturation of the βII-Spectrin scaffold to a lattice-like periodic organisation and the maintenance of the MPS.

In this study, we evaluate the axonal segments in the middle 50% of the DRG axon to investigate the establishment of long-range periodic order and the typical spacing of the βII-Spectrin MPS. We find that βII-Spectrin is already present at the axonal cortex by DIV1, though its organisation is weakly periodic. The scaffold matures progressively with development with the degree of periodicity increasing and the variability of the spectrin spacing concomitantly decreasing and converging to ~185 nm by DIV 6 (Fig 1A-E). However, there is no obvious change in the amount of βII-Spectrin (Fig S1A) between DIVs indicating re-modelling of early recruited spectrin to a periodic organisation with long-range order. These data also indicate a more rapid development of the MPS in embryonic DRG neurons compared to hippocampal (Zhong *et al.*, 2014) and cortical neurons (Hofmann *et al.*, 2022).

The progressive maturation of the MPS was coincident with a reduction in the axonal diameter. The role of the MPS in regulating axonal diameter has been demonstrated previously(Costa *et al.*, 2020; Wang *et al.*, 2020) and our data suggests maturation of the MPS results in increased radial constriction possibly due to the recruitment of myosin and stabilisation of the F-actin rings. Axonal pre-tension also increases modestly with the increase in the periodic organisation, though it is interesting to note that even at DIV1 there is substantial pre-tension. Axonal pre-tension has been previously associated with spectrin (Krieg *et al.*, 2014) and the non-periodic organisation of spectrin in non-neuronal cells are also load-bearing (Lee and Discher, 2001; Smith *et al.*, 2018; Ghisleni *et al.*, 2020). The weakly periodic spectrin organisation observed at DIV1 may form a networked scaffold that supports the axonal pre-stress. However, cytoskeletal components are also likely to contribute significantly as load-bearing structures in the axon (Mutalik *et al.*, 2018; Leterrier and Pullarkat, 2022; Ghose and Pullarkat, 2023).

Acute depolymerisation of microtubules led to the destabilisation of the MPS at all developmental stages (Fig. 2). This suggests a microtubule-dependent MPS maintenance function. Similar observations have been made in hippocampal neurons (Zhong *et al.*, 2014). Conversely, in *Drosophila* neurons, periodic actin is proposed to maintain microtubule alignment and stability (Qu *et al.*, 2017). In *C. elegans*, loss of spectrin reduces the length of axonal microtubules in some neurons (Krieg *et al.*, 2017). To probe the contribution of microtubule to MPS formation further, we subjected early axons to a low chronic dose of microtubule modifying drugs (Fig. 3). As with the acute treatment, continuous exposure to a low dose of Noco from 16h after seeding, resulted in compromised MPS in both DIV 2 and DIV4. Surprisingly, and in contrast to acute treatment with taxol, chronic stabilisation of microtubules in early axons also destabilised the MPS at both DIV 2 and 4. These observations suggest the requirement of microtubule dynamics in the establishment

of the βII-Spectrin MPS. Apart from stabilising microtubule, taxol can also promote microtubule growth and nucleation, these changes may influence MPS development (Witte *et al.*, 2008; Verma *et al.*, 2016). In epithelial lateral membranes, the mobility of spectrin domains is sensitive to microtubule depolymerisation (Jenkins *et al.*, 2015), however, it is unclear if an analogous or distinct mechanism is involved in axonal MPS development.

Acute depolymerisation but not stabilisation of F-actin resulted in the loss of βII-spectrin MPS across all stages of early development as has also been demonstrated in both young and older axons (Zhong *et al.*, 2014; Han *et al.*, 2017; Qu *et al.*, 2017). A key role of F-actin, in the form of the circumferential rings, involves the crosslinking of spectrin heterotetramers into the longitudinal periodic arrangement seen in axons(Xu *et al.*, 2013; Vassilopoulos *et al.*, 2019). Further, subplasmalemmal F-actin is likely to facilitate the cortical recruitment of spectrin heterotetramers early in development and initiate the organisation of the crosslinked spectrin scaffold. Inhibition of actin nucleation early in development (DIV2, 4) resulted in disruption of the MPS. However, acute inhibition of actin nucleation at later stages (DIV 6) did not affect the established MPS. This suggests that dynamically nucleating actin networks in early development are required for MPS development but the contribution of fresh actin nucleation-dependent turnover, over the timescales evaluated, is not necessary for MPS maintenance.

FRAP experiments revealed that βII-spectrin gets increasingly stabilised at the axonal cortex with development, consistent with previous observations in hippocampal neurons (Xu *et al.*, 2013). We show that a significant component of the cortical recruitment of βII-spectrin is via interactions with F-actin, though this dependency reduces as the MPS matures. As βII-spectrin but not αII-spectrin can directly bind F-actin (Li and Bennett, 1996) , the latter is expected to drive the interactions of the spectrin heterotetramer with cortical actin.

To further probe subplasmalemmal recruitment of βII-spectrin, we developed a model of differentiated human SH-SY5Y cells engineered to lack βII-spectrin. By expressing βII-spectrin spectrin variants in this system, we established the essential roles of the membrane interacting PH-domain and the actin-binding domain in the development of the MPS. These data are consistent with observations in mouse neurons (Zhou *et al.*, 2022). FRAP analysis of mutant spectrin revealed that the actin-binding domain of βII-spectrin is required for its recruitment and stabilisation at the axonal cortex. Additionally, interactions with the plasma membrane lipids via the PH-domain also contribute to subplasmalemmal confinement.

In fibroblasts, actomyosin activity can drive the transition from a diffuse orientation of βII-spectrin to a periodic configuration (Ghisleni *et al.*, 2024). In contrast, blebbistatin treatment does not affect the MPS in mature neurons though it increases the axonal diameter by reducing radial contractility (Costa *et al.*, 2020; Wang *et al.*, 2020). However, as early DRG axons are actively contractile (Mutalik *et al.*, 2018) there may be a role for actomyosin contractility in driving the reorganisation of βII-spectrin to a periodic scaffold.

This work highlights the dynamic maturation of the βII-spectrin MPS in early development. Dynamics of the microtubule and the actin cytoskeletons contribute to the development of the MPS. Interactions with F-actin and the membrane drive the early subplasmalemmal confinement of βII-spectrin, which subsequently matures to

an extended scaffold with long-range periodic order and whose maintenance is dependent on both stable F-actin and microtubules.

REFERENCES

Albrecht, D, Winterflood, CM, Sadeghi, M, Tschager, T, Noé, F, and Ewers, H (2016). Nanoscopic compartmentalization of membrane protein motion at the axon initial segment. J Cell Biol 215, 37–46.

Costa, AR, Sousa, SC, Pinto-Costa, R, Mateus, JC, Lopes, CD, Costa, AC, Rosa, D, Machado, D, Pajuelo, L, Wang, X, *et al.* (2020). The membrane periodic skeleton is an actomyosin network that regulates axonal diameter and conduction. eLife. Available at: https://elifesciences.org/articles/55471/figures.

Cousin, MA, Creighton, BA, Breau, KA, Spillmann, RC, Torti, E, Dontu, S, Tripathi, S, Ajit, D, Edwards, RJ, Afriyie, S, *et al.* (2021). Pathogenic SPTBN1 variants cause an autosomal dominant neurodevelopmental syndrome. Nat Genet 53, 1006–1021.

D'Este, E, Kamin, D, Velte, C, Göttfert, F, Simons, M, and Hell, SW (2016). Subcortical cytoskeleton periodicity throughout the nervous system. Sci Rep 6, 22741.

Dubey, S, Bhembre, N, Bodas, S, Veer, S, Ghose, A, Callan-Jones, A, and Pullarkat, P (2020). The axonal actin-spectrin lattice acts as a tension buffering shock absorber. eLife 9, e51772.

Ghisleni, A, Bonilla-Quintana, M, Crestani, M, Lavagnino, Z, Galli, C, Rangamani, P, and Gauthier, NC (2024). Mechanically induced topological transition of spectrin regulates its distribution in the mammalian cell cortex. Nat Commun 15, 5711.

Ghisleni, A, Galli, C, Monzo, P, Ascione, F, Fardin, M-A, Scita, G, Li, Q, Maiuri, P, and Gauthier, NC (2020). Complementary mesoscale dynamics of spectrin and acto-myosin shape membrane territories during mechanoresponse. Nat Commun 11, 5108.

Ghose, A, and Pullarkat, P (2023). The role of mechanics in axonal stability and development. Semin Cell Dev Biol 140, 22–34.

Hammarlund, M, Jorgensen, EM, and Bastiani, MJ (2007). Axons break in animals lacking β-spectrin. J Cell Biol 176, 269–275.

Han, B, Zhou, R, Xia, C, and Zhuang, X (2017). Structural organization of the actin-spectrin–based membrane skeleton in dendrites and soma of neurons. Proc Natl Acad Sci 114, E6678–E6685.

He, J, Zhou, R, Wu, Z, Carrasco, MA, Kurshan, PT, Farley, JE, Simon, DJ, Wang, G, Han, B, Hao, J, *et al.* (2016). Prevalent presence of periodic actin–spectrin-based membrane skeleton in a broad range of neuronal cell types and animal species. Proc Natl Acad Sci 113, 6029–6034.

Ho, J, Tumkaya, T, Aryal, S, Choi, H, and Claridge-Chang, A (2019). Moving beyond P values: data analysis with estimation graphics. Nat Methods 16, 565–566.

Hofmann, M, Biller, L, Michel, U, Bähr, M, and Koch, JC (2022). Cytoskeletal assembly in axonal outgrowth and regeneration analyzed on the nanoscale. Sci Rep 12, 14387.

Huang, CY-M, Zhang, C, Ho, TS-Y, Oses-Prieto, J, Burlingame, AL, Lalonde, J, Noebels, JL, Leterrier, C, and Rasband, MN (2017a). αII Spectrin Forms a Periodic Cytoskeleton at the Axon Initial Segment and Is Required for Nervous System Function. J Neurosci 37, 11311–11322.

Huang, CY-M, Zhang, C, Zollinger, DR, Leterrier, C, and Rasband, MN (2017b). An αII Spectrin-Based Cytoskeleton Protects Large-Diameter Myelinated Axons from Degeneration. J Neurosci 37, 11323–11334.

Jenkins, PM, He, M, and Bennett, V (2015). Dynamic spectrin/ankyrin-G microdomains promote lateral membrane assembly by opposing endocytosis. Sci Adv 1, e1500301.

Krieg, M, Dunn, AR, and Goodman, MB (2014). Mechanical control of the sense of touch by β-spectrin. Nat Cell Biol 16, 224–233.

Krieg, M, Stühmer, J, Cueva, JG, Fetter, R, Spilker, K, Cremers, D, Shen, K, Dunn, AR, and Goodman, MB (2017). Genetic defects in β-spectrin and tau sensitize C. elegans axons to movement-induced damage via torque-tension coupling. eLife 6, e20172.

Lee, JC-M, and Discher, DE (2001). Deformation-Enhanced Fluctuations in the Red Cell Skeleton with Theoretical Relations to Elasticity, Connectivity, and Spectrin Unfolding. Biophys J 81, 3178–3192.

Leterrier, C, and Pullarkat, PA (2022). Mechanical role of the submembrane spectrin scaffold in red blood cells and neurons. J Cell Sci 135, jcs259356.

Li, X, and Bennett, V (1996). Identification of the Spectrin Subunit and Domains Required for Formation of Spectrin/Adducin/Actin Complexes *. J Biol Chem 271, 15695–15702.

Lorenzo, DN, Badea, A, Zhou, R, Mohler, PJ, Zhuang, X, and Bennett, V (2019). βII-spectrin promotes mouse brain connectivity through stabilizing axonal plasma membranes and enabling axonal organelle transport.

Mutalik, SP, Joseph, J, Pullarkat, PA, and Ghose, A (2018). Cytoskeletal Mechanisms of Axonal Contractility. Biophys J 115, 713–724.

Nishimura, Y, Shi, S, Zhang, F, Liu, R, Takagi, Y, Bershadsky, AD, Viasnoff, V, and Sellers, JR (2021). The formin inhibitor SMIFH2 inhibits members of the myosin superfamily. J Cell Sci 134, jcs253708.

Qu, Y, Hahn, I, Webb, SED, Pearce, SP, and Prokop, A (2017). Periodic actin structures in neuronal axons are required to maintain microtubules. Mol Biol Cell 28, 296–308.

Ran, FA, Hsu, PD, Wright, J, Agarwala, V, Scott, DA, and Zhang, F (2013). Genome engineering using the CRISPR-Cas9 system. Nat Protoc 8, 2281–2308.

Smith, AS, Nowak, RB, Zhou, S, Giannetto, M, Gokhin, DS, Papoin, J, Ghiran, IC, Blanc, L, Wan, J, and Fowler, VM (2018). Myosin IIA interacts with the spectrin-actin membrane skeleton to control red blood cell membrane curvature and deformability. Proc Natl Acad Sci 115, E4377–E4385.

Unsain, N, Bordenave, MD, Martinez, GF, Jalil, S, von Bilderling, C, Barabas, FM, Masullo, LA, Johnstone, AD, Barker, PA, Bisbal, M, *et al.* (2018). Remodeling of the Actin/Spectrin Membrane-associated Periodic Skeleton, Growth Cone Collapse and F-Actin Decrease during Axonal Degeneration. Sci Rep 8, 3007.

Vassilopoulos, S, Gibaud, S, Jimenez, A, Caillol, G, and Leterrier, C (2019). Ultrastructure of the axonal periodic scaffold reveals a braid-like organization of actin rings. Nat Commun 10, 5803.

Verma, S, Kumar, N, and Verma, V (2016). Role of paclitaxel on critical nucleation concentration of tubulin and its effects thereof. Biochem Biophys Res Commun 478, 1350–1354.

Wang, G, Simon, DJ, Wu, Z, Belsky, DM, Heller, E, O'Rourke, MK, Hertz, NT, Molina, H, Zhong, G, Tessier-Lavigne, M, *et al.* (2019). Structural plasticity of actin-spectrin membrane skeleton and functional role of actin and spectrin in axon degeneration. eLife 8, e38730.

Wang, T, Li, W, Martin, S, Papadopulos, A, Joensuu, M, Liu, C, Jiang, A, Shamsollahi, G, Amor, R, Lanoue, V, *et al.* (2020). Radial contractility of actomyosin rings facilitates axonal trafficking and structural stability. J Cell Biol 219, e201902001.

Wernert, F, Moparthi, SB, Pelletier, F, Lainé, J, Simons, E, Moulay, G, Rueda, F, Jullien, N, Benkhelifa-Ziyyat, S, Papandréou, M-J, *et al.* (2024). The actin-spectrin submembrane scaffold restricts endocytosis along proximal axons. Science 385, eado2032.

Witte, H, Neukirchen, D, and Bradke, F (2008). Microtubule stabilization specifies initial neuronal polarization. J Cell Biol 180, 619–632.

Xu, K, Zhong, G, and Zhuang, X (2013). Actin, Spectrin, and Associated Proteins Form a Periodic Cytoskeletal Structure in Axons. Science 339, 452–456.

Zhong, G, He, J, Zhou, R, Lorenzo, D, Babcock, HP, Bennett, V, and Zhuang, X (2014). Developmental mechanism of the periodic membrane skeleton in axons. eLife 3, e04581.

Zhou, R, Han, B, Nowak, R, Lu, Y, Heller, E, Xia, C, Chishti, AH, Fowler, VM, and Zhuang, X (2022). Proteomic and functional analyses of the periodic membrane skeleton in neurons. Nat Commun 13, 3196.

Zhou, R, Han, B, Xia, C, and Zhuang, X (2019). Membrane-associated periodic skeleton is a signaling platform for RTK transactivation in neurons. Science 365, 929–934.

Estimation Stats. Available at: https://www.estimationstats.com

AUTHOR CONTRIBUTIONS

Conceptualization: S.B. and A.G.; Investigation and formal analysis (all experiments other than laser ablation experiments): S.B.; Investigation and formal analysis (laser ablation experiments): S.B. and A.M.; Methodology and resources: S.B., A.M., P.P. and A.G.; Writing – original draft: S.B. and A.G.; Writing – review and editing: S.B., A.M., P.P. and A.G; Funding Acquisition: A.G., P.P.

All authors gave final approval for publication and agreed to be held accountable for the work performed therein.

FUNDING

This work was supported by grant no.: IA/TSG/20/1/600137 from DBT-Wellcome Trust India Alliance, grant no.: DST/INT/Portugal/P-04/2021(G) from the Dept. of Science & Technology, Govt. on India and intramural funds from IISER Pune.

ACKNOWLEDGEMENTS

The IISER Pune Microscopy Facility is acknowledged for access to imaging systems and software. We thank Dr. Sayantan Majumdar, RRI Bengaluru for lending the high-speed camera for laser ablation experiments.